Synthesis and sintering of nanocrystalline Ce3+ - doped yttria nanoparticles prepared by precipitation method

Nibu Puthenpurayil Govindan (nibu.puthenpurayil@tnuni.sk)
FUNGLASS
Monika Michálková
FUNGLASS
Peter Švančárek
FUNGLASS
Róbert Klement
FUNGLASS
Dušan Galusek
FUNGLASS

Research Article

Keywords: Y2O3, Ceramic, Precipitation, EBSD

Posted Date: July 7th, 2020

DOI: https://doi.org/10.21203/rs.3.rs-40087/v1

Abstract

Cerium doped yttrium oxide (Y 1.999 Ce 0.001 O 3 , Y 1.995 Ce 0.005 O 3, Y 1.99 Ce 0.01 O 3) nanoparticles have been synthesized by precipitation method with ammonium hydroxide as a precipitation agent. Partly agglomerated powders with the primary size of Y 2 O 3 nanoparticles with the mean size of ~ 55 nm and cubic crystal structure were prepared. The green compacts were prepared from alcoholic suspension with PEG as a dispersant by vacuum-pressure filtration. The green bodies reached relative density over 43 % while relative density of sintered specimens (1550 °C/3 h) were in all cases close to 98 %. All sintered ceria doped samples displayed dense microstructure with closed porosity and monomodal grain size distribution. The samples exhibit light emission in the blue wavelength range, centred at 430 nm.

1. Introduction

Yttria ceramics have many potential applications such as lighting and display application [1, 2], IR windows, laser host material [3, 4], and high temperature resistant windows [5]. RE/Yb co-doped Y_2O_3 transparent ceramics (RE = Er^{3+}, Pr^{3+} and Tm^{3+}), exhibited very efficient NIR-visible up conversion, therefore the optical properties of Y_2O_3 ceramics doped with rare earth ions are of special interest for solid state lasers and scintillators [6–9].

Nowadays, Y_2O_3 based ceramics are sintered by different methods such as hot pressing, conventional pressureless sintering, and spark plasma sintering [10–14]. However, preparation of transparent yttria ceramics is usually rather difficult, and preparation of high quality green body is crucial. It should be noted that powders with small particle size, monomodal particle size distribution, and low degree of agglomeration are crucial for the preparation of yttria based transparent ceramics [15, 16]. Using nanoparticles as starting materials creates potential for fabrication of ceramics, which is not only transparent but is prepared at considerably lower temperatures of sintering [17–23]. Moreover, better mechanical properties ascribed to materials with the nanosized microstructure, compared to their coarser grained counterparts with microsized microstructure, can be achieved.

Yttria nanopowders with a particle size ranging from 20 to 100 nm have been prepared by different techniques such as combustion synthesis [17–19], sol–gel [20, 21], electrospray pyrolysis [22] and co-precipitation [23]. Most of the above mentioned methods involve many steps and complicated procedure. Precipitation method utilizing inorganic salts as raw materials has shown its merits for producing yttria powders. Moreover, this technique includes fewer simple steps and requires lower cost raw materials. In 2006 Wen et al. [24] reported the preparation of easily sinterable Y_2O_3 nanopowders of excellent purity by calcination of the yttrium hydroxide at 1100 ºC for 4 h. Additionally, transparent yttria ceramics were fabricated from the nano Y_2O_3 powders by vacuum sintering at 1700 ºC for 4 h. However, nanopowders have higher tendency to agglomerate than microsized powders because of extremely high specific surface area [20, 22, 25]. The agglomeration is caused by attractive van der Walls forces among nanosized particles. The high surface area and nanosized microstructure leads to formation of

agglomerates. Powder agglomeration promotes the emergence of large inter-agglomerate pores and heterogeneous particle distribution in the green body. Such internal defects lead to lower densities of the green bodies, and usually cannot be eliminated during sintering, effectively preventing preparation of transparent ceramics [26].

Colloidal process is a wet chemical process usually involving the addition of dispersant in order to manipulate interparticle forces within the suspending medium [27, 28], to overcome the agglomeration ability of the suspension. Colloidal processes include slip casting, injection moulding, tape casting and gel casting [29, 30]. However, in comparison to other ceramic materials there are only few works dealing with colloidal processing of Y_2O_3 ceramics. Uckikoshi *et al* [31] used poly-ethylene imine (PEI) as a dispersant to stabilize the Y_2O_3 nano-sized suspensions. Mouzon et al [32] developed suspensions with 23 vol % of Y_2O_3 nanopowder with a specific area of 17.2 m^2/g. Jiao *et al* [33] prepared transparent yttria ceramics using nano-sized yttria powder and using tri ammonium citrate as the dispersant. Jin *et al* [34] found Dolapix CE64 was the most effective dispersant for de-agglomeration and stabilisation of yttria suspension when compared with Dispex A40 and Darvan C-N.

If there is only limited number of publications dealing with colloidal processing of yttria nanopowders, there are even less, which report on preparation of Ce^{3+} doped yttria nanopowders and their use in fabrication of polycrystalline yttria ceramics. Kruk fabricated Ce^{3+} doped yttria transparent ceramics with very large grain size (4–28 μm) using a Ce^{3+} doped yttria powder prepared by arc melting method [35]. Zhidkov *et al.* [36] studied the increase of the optical transparency in the post-annealed Y_2O_3 ceramics doped with 5 mol % CeO_2. To the best of our best knowledge there are no reports dealing with preparation of Ce^{3+} doped Y_2O_3 nanopowders by the precipitation process, using ammonium hydroxide as the precipitation agent, and its application for preparation of a highly dense yttria ceramics with fine grained microstructure.

The present study fills the gap. The green compacts were successfully prepared by vacuum-pressure filtration of an alcoholic suspension stabilized with polyethylene glycol and pressure less sintered to almost fully dense polycrystalline yttria ceramics with fine-grained microstructure.

2. Materials And Methods

To prepare yttria nanoparticles with three different ceria doping levels, 0.001 mol % (denoted as Ce-1), 0.005 mol % (Ce-2), and 0.01 mol % (Ce-3), 0.1 M aqueous nitrate solution of Y^{3+} was prepared by dissolving commercial Y_2O_3 (99.9%, Treibacher industries, Austria) in nitric acid (65%) and water under stirring and heating at 100 °C. The solution was then diluted by deionised water to 0.1 M. The 0.1 M solution of Ce^{3+} was prepared by dissolving cerium nitrate (99.9%, Alfa Aesar, USA) in deionized water. The mixed metal nitrate solution was added dropwise with the use of a peristaltic pump at 5.0 ml/min, into a 0.5 M ammonium hydroxide solution, under continuous rapid stirring, ensuring there was sufficiently high excess of ammonia (maintaining pH ~ 12 throughout the process). The reaction was

completed in 24 h and the clear solution turned to opaque white slurry. After 12 h of aging, the slurry was vacuum filtrated and the white precipitate was washed with deionised water. The washed precipitate was dried overnight in the air at 100 °C. The dried precipitate was crushed and ground in an agate mortar with pestle, and calcined in air for 3 h at 700 °C (heating rate 5 °C/min).

Decomposition of dried precursor, as well as the crystallization behaviour of the prepared Y_2O_3 precipitate, was studied using Netzsch STA 449 F1 Jupiter DTA/DSC in DSC mode, equipped with cooling accessory. The measurement was carried out at the heating rate of 5 °C/min in the temperature range from 20 °C to 1000 °C. The phase composition was determined by X-ray powder diffraction (XRD) using Panalytical Empyrean DY1098 diffractometer, operated at 40 kV and 45 mA with Cu Kα radiation (λ = 0.15405 nm). The data were acquired over a 2θ range of 10–70 ° (step size 0.01 °, 50 s/ step). The data were evaluated using the Panalytical High Score Plus software package with the PDF4 + database. Particle size and morphology of prepared particles were examined by scanning electron microscopy (JEOL JSM-7600 F / EDS / WDS / EBSD).

The precipitation method led to severe agglomeration of ceria doped yttria powder. The powder was therefore subjected to de-agglomeration before the preparation of green compacts. The Ce^{3+} doped Y_2O_3 isopropanol suspension with 30 vol. % of solid loading was dispersed by ultrasonication (Bandelin UV2200) for 32 min with polyethylene glycol (Vanderbilt Minerals, Germany) as a dispersant (2 wt %, related to the weight of yttria nanopowder). Dynamic light scattering (DLS) was employed to determine the particle size distribution in the suspensions using a particle size analyser (Nano Brook 90Plus, Brookhaven, NY, USA); the measured suspensions were diluted to ∼ 100 ppm by addition of isopropyl alcohol. Stability of yttria suspension and the optimal amount of dispersant was evaluated by sedimentation test. 30 vol. % Y_2O_3 suspensions with 7 different polyethylene glycol concentrations (0.5–3.5 wt. %) was used for the sedimentation test. The sedimentation volume was determined by keeping 30 ml of each suspension in a stoppered measuring cylinder and stored undisturbed at room temperature. The sedimentation height was noted after 24 h. Green compacts were prepared by the vacuum - pressure filtration of the ultrasonically de-agglomerated yttria suspension. The vacuum - pressure filtration was performed in a special die with a diameter of 15 mm. The suspension (30 vol. % solid loading) was poured into the die and a pressure of 50 MPa was applied by a uniaxial hydraulic press. The isopropyl alcohol from the suspension was drained through massive perforated metal bottom with a polymeric membrane (pore size 0.2 μm). The density of green samples was determined by geometrical method. The green body was air-calcined at 900 °C to remove the organic and then sintered at 1550 °C for 3 h at a heating rate of 10 °C/min. Relative density of sintered samples was determined by Archimedes principle in deionised water. At last, the Ce^{3+} - doped Y_2O_3 ceramics samples were ground and polished into 1.0 mm thickness for further characterizations. EBSD analysis were performed using a scanning electron microscopy (JEOL JSM-7600 F / EDS / WDS / EBSD) at the accelerating voltage 15 kV with an EDAX Trident analysing system containing a Digi view 3 EBSD-camera. Energy-dispersive X-ray spectrometry (EDXS) was performed with a standard using acceleration voltage 15 kV. Before the measurement the specimens where plasma coated with Au/Pd alloy for 3 seconds. The mean grain size

of Ce^{3+} - doped Y_2O_3 ceramics was determined by linear intercept method, measuring at least 300 intercepts (software LINCE, TU Darmstadt, Germany), and using the correction factor 1.56 [37].

The excitation and emission fluorescence spectra were measured using Fluorolog FL3-21 spectrometer (Horiba, Ltd., Japan) with Xe-lamp (450 W) as an excitation source. The luminescence spectra of studied samples were recorded at room temperature.

3. Results And Discussion

3.1. TG-DTA analysis of the precursor powder

Figure 1 presents the results of DSC and related TG analysis of prepared $[Y(NO_3)_3 \cdot xY(OH)_3 \cdot yH_2O]$ precipitate. Broad endothermic centred at 143 °C and 277 °C are related to dehydration of free and physically adsorbed molecular water [38, 39]. The dehydration of chemisorbed and combined water from $Y(OH)_3$ and α-$Y(OH)_3$ is represented by the endothermic effect at 330 °C. Due to the presence of HNO_3 during the dissolution of yttria, basic yttrium hydroxyl-nitrate complex $[Y_2(NO_3)_3 \cdot xY(OH)_3 \cdot yH_2O]$ is formed [40, 41]. Decomposition of such complexes takes place at about 535 °C [42]. Consequently, as confirmed by the TG/ DSC record, decomposition of prepared yttria precursor is completed at 600 °C. No more exothermic or endothermic effects were detected at higher temperatures. The calcination of Y_2O_3 powder prepared by precipitation was therefore carried out at 700 °C.

3.2. Powder characteristics

The phase evaluation of the Ce^{3+} doped Y_2O_3 powder was carried out using X-ray powder diffraction (XRD) technique. Figure 2 shows the diffraction patterns of Ce^{3+} doped Y_2O_3 powder calcined at 700 °C. The diffraction peaks confirm the formation of a single phase, pure cubic yttria, with the Ia-3 space group (JCPDS Card No.83–0927). The primary particle size of prepared nanoparticles, as determined from the Scherer equation, was approximately 55 nm. Due to the very low concentration of ceria in doped yttria powder no change or shift of peak positions in the XRD pattern was observed. Hence, change of the crystal lattice is so small that it could not be detected by XRD.

3.3. Microstructure analysis and particle size distribution of yttria powders

Figure 3 shows the SEM micrographs of synthesized Ce^{3+} doped Y_2O_3 particles calcined at 700 °C for 3 h. All ceria doped samples are agglomerated; most particles are spherical with an average particle size of 55 nm, which is in accord with the X-ray diffraction data. Both morphology and size of the nanoparticles prepared in the present study are similar to the results in the reference [43]. All ceria doped samples show comparable particle size. Doping of yttria powder by ceria did not have any significant influence on

particle size and distribution. In order to deagglomerate the powder high power ultrasonication has been performed. The results are shown in Fig. 4.

Figure 4 summarizes the changes in particle size distribution of ceria doped yttria nanoparticles in alcoholic suspension with the sonication time. Extension of the ultrasonication time results in significant reduction of the mean particle size. High agglomeration ability of Y_2O_3 powder is visible even after 1 min of ultrasonication where the particle size distribution is in micro - range (1-2 μm). The best results were achieved after 32 minutes of sonication. Ultrasonication of alcoholic yttria suspension led to an average particle size of 200 nm; however, both the SEM examination and the results of X-ray powder diffraction indicate the primary particle size around 55 nm. This clearly shows that the powder was not completely de-agglomerated down to primary particles, and hard agglomerates with the diameter of about 200 nm were still present.

3.4. Sedimentation tests

To find out the optimal concentration of PEG in suspension, sedimentation tests were utilized. Figure 5 displays the final sedimentation volume of the concentrated (30 vol. %) suspensions of Ce^{3+} doped Y_2O_3 nanoparticles at 7 different concentrations of polyethylene glycol (PEG) determined after 24 h of sedimentation time. The sedimentation analysis enables the selection of the optimum polyethylene glycol weight fraction in the colloidal suspension before pressure filtration. The de-agglomeration and dispersion of ceramic powder processing are crucial for obtaining of a high density and pore free material. Any inhomogeneity in the suspension, e.g. segregation, density gradients or presence of agglomerates present in the suspension, result in decreased stability of the suspension and its fast sedimentation [44]. All ceria doped powders prepared in this study show similar sedimentation behaviour: the suspension achieved the lowest sedimentation rate when the concentration of polyethylene glycol (PEG) was 2.0 wt. %, related to weight of yttria powder. The suspensions with 2.0 wt. % of polyethylene glycol (PEG) were therefore used for pressure filtration. The relative density of the pressure-casted green body reached a maximal value of 43%.

3.5. Characterisation of the samples after sintering

Figure 6 shows the XRD patterns of Y_2O_3:Ce^{3+} ceramics sintered at 1550 °C for 3 h in air. The samples are well crystalized and contain a pure cubic Y_2O_3 as the only crystalline phase.

Figure 7 shows the fracture surfaces of ceria doped yttria ceramics prepared by pressure filtration method and sintered at 1550 °C for 3 h. It can be noted that all ceria doped samples were sintered to high density containing limited amount of closed pores, providing a material which can be further densified by hot isostatic pressing. Table 1 summarizes the relative densities of all Ce^{3+} doped yttria samples after sintering at 1550 °C. All Ce^{3+} doped yttria ceramics prepared in this study reached the density close to 98 %. With increasing the Ce^{3+} concentration the density slightly increased. More detailed investigation of the influence of Ce^{3+} doping on sinterability of yttria nanopowders prepared in this study is in progress.

Table 1

Relative densities of Ce^{3+} doped yttria ceramic prepared by vacuum pressure filtration method, sintered at 1550 °C for 3 h.

Sample	Relative density
Ce-1	97.9 ± 0.5%
Ce-2	98.4 ± 0.5%
Ce-3	98.6 ± 0.5%

Figure 8 shows the microstructure of polished ceria doped yttria ceramics prepared by vacuum pressure filtration, sintered at 1550 °C for 3h. The micrographs confirm that all samples are relatively coarse-grained, with median grain size ranging between 2 and 6 μm. However, these results still represent a significant microstructure refinement when compared with the works of Kruk who prepared Ce^{3+} doped yttria ceramics with the grain size up to 28 μm [35], and the work of Huang et al, where undoped yttria ceramics sintered to high density with the grain size (30 μm) was prepared [43]. Ceria doping did not have any influence on the microstructure of the sintered ceramics, and the histograms showing the grain size distributions of all Ce^{3+} doped yttria ceramics were almost identical.

Figure 9 A shows the emission spectra of Ce^{3+} doped yttria ceramics sintered at 1550 °C/3h. The material Ce-1 exhibits very weak emissions with the maximum intensity at 410 nm and 487 nm, respectively. Ce-2 shows a broad emission centred at 434 nm, while the maximum of the Ce-3 emission is at 423 nm. The broad emission bands are attributed to the electron transition of Ce^{3+}, which can be assigned to the $^5d_1 \rightarrow {}^2F_{7/2}$ and $^5d_1 \rightarrow {}^2F_{5/2}$ energy level transitions of Ce^{3+} ions from the lowest 5d level to the ground 4f levels. It was reported that the excitation and emission spectra of Ce^{3+} - doped compounds mainly depend on the crystalline environment around the Ce^{3+} ions [45, 46]. It is well established that when Ce^{3+} is localised in a single lattice site, the asymmetry in the emission of Ce^{3+} corresponds to the transitions from the lowest 5d excited state to the $^2F_{5/2}$ and $^2F_{7/2}$ spin-orbit split of 4f ground states [47, 48]. Figure 9b shows the normalized emission intensities. The Ce-1 shows two broad emissions centred at 410 nm and 487 nm. This spectrum is almost identical to the emission spectra of undoped yttria, and is attributed to energy transfers at structural defects in the yttria crystal lattice [49]. Contribution of the ceria emission is negligible in the Ce-1. Less pronounced peak splitting is observed also in Ce-2, and Ce-3, with the intensity of the band centred at 487 nm decreased with increasing ceria content. The intensity of the band centred at 410 nm is correlated with the increasing content of the Ce^{3+} ions in the yttria crystal lattice. These measured emission spectra are similar to that of the LuAG: Ce single crystal and match well the requirements for photo-detectors, or scintillators [50, 51].

4. Conclusions

Ce^{3+} doped Y_2O_3 nanoparticles with various contents of doping were synthesized by precipitation method using ammonium hydroxide as the precipitation agent. Partly agglomerated powders with the primary size of Y_2O_3 nanoparticles 55 nm and cubic crystal structure were prepared by calcination of precipitates at 700 °C. The relative density of green compacts prepared by vacuum-pressure filtration of isopropanol-based suspensions was ~ 43%. The relative density of sintered Ce^{3+} doped yttria samples was in all cases close to 98%. Particle size distributions of all prepared ceramics were almost identical, and the size of yttria grains ranged between 2–6 μm. Ce^{3+} doping does not result in any significant change in the particle size distribution. Ce-doped ceramics emits in blue wavelength region, with the emission intensity increasing with increasing ceria doping.

Declarations

Acknowledgement

The financial support of this work by the grant VEGA 2/0026/17 is gratefully acknowledged. This project is part of dissemination activities of the project Centre for functional and surface functionalized glass (acronym CEGLASS), ITMS code 313011R453, operational program Research and innovation, co-funded from the European Regional Development Fund.

References

[1] Putkonen M, Sajavaara T, Johansson LS, *et al*. Low-Temperature ALE Deposition of Y_2O_3 Thin Films from β-Diketonate Precursors. *Chem Vap Deposition* 2001, **7:** 44–50.

[2] Möslang M, Adelhelm C, Heidinger R. Innovative materials for energy technology, *Mater Re*s 2008, **99:** 1045–1054.

[3] Podowitz SR, Gaumé R, Feigelson RS. Effect of Europium Concentration on Densification of Transparent Eu:Y_2O_3 Scintillator Ceramics Using Hot Pressing.
J Am Ceram Soc 2010, **93:** 82–88.

[4] Ivanov M, Kopylov Y, Kravchenko V, *et al*. Optical, luminescent and laser properties of highly transparent ytterbium doped yttrium lanthanum oxide ceramics. *Opt Mater 2015*, **50:** 15–20.

[5] SellersD, Roy D. Method for making heat resistant transparent optical elements. U.S. patent 3768990, Oct.1973.

[6] Song X, Xie M, Zhou F, *et al.* High-temperature thermal properties of yttria fully stabilized zirconia ceramics. *J Rare Earths* 2011, **29:** 155–159.

[7] Hou X, Zhou S, Jia T, *et al.* White light emission in $Tm^{3+}/Er^{3+}/Yb^{3+}$ tri-doped Y_2O_3 transparent ceramic. *J Alloys Compd* 2011, **509:** 2793–2796.

[8] Poma PY, Kumar KU, Vermelho MD, *et al.* Luminescence and thermal lensing characterization of singly Eu^{3+} and Tm^{3+} doped Y_2O_3 transparent ceramics. *J Lumin* 2015, **161:** 306–312.

[9] Hou X, Zhou S, Jia T, *et al.* Investigation of up-conversion luminescence properties of RE / Yb co-doped Y_2O_3 transparent ceramic (RE = Er , Ho , Pr , and Tm). *Physica B Condens Matter* 2011, **406:** 3931–3937.

[10] Huo D, Zheng Y, Sun X, *et al* .Preparation of transparent Y_2O_3 ceramic by slip casting and vacuum sintering. *J Rare Earths* 2012, **30:** 57–62.

[11] Zhou J, Chen Y, Lei R, *et al*. Excellent photoluminescence and temperature sensing properties in Ho^{3+}. *Ceram Int.* 2019, **45:** 7696–7702.

[12] Huang Z, Guo W, Liu Y, *et al.* Synthesis of Nd:Y_2O_3 nanopowders leading to transparent ceramics. *Mater Chem Phys* 2011, **128:** 44–49.

[13] Jin L, Zhou G, Shimai S, *et al.*ZrO_2 -doped Y_2O_3 transparent ceramics via slip casting and vacuum sintering. *Eur Ceram Soc* 2010, **30:** 2139–2143.

[14] Futami F, Yanagida T, Fujimoto Y, *et al.*A. Yoshikawa, T. Goto, Optical and scintillation properties of Sc_2O_3, Y_2O_3 and Lu_2O_3 transparent ceramics synthesized by SPS method. *Radiat Meas.* 2013, 55: 136–140.

[15] Abdelrazek K, Advanced Sintering of Nano-Ceramic Materials, *Ceramic Materials - Progress in Modern Ceramics,* Feng Shi, Eds. Janeza Trdine Croatia 2012: 65-82

[16] Chen IW, Wang XH, Sintering dense nanocrystalline ceramics without final-stage grain growth . *Nature* 2000, **404:** 168–171.

[17] Tessari G, Bettinelli M, Speghini A, *et al.* Synthesis and optical properties of nanosized powders : lanthanide-doped Y_2O_3. *Appl Surf Sci* 1999, **144:** 686–689.

[18] Mangalaraja RV, Mouzon J, Hedström P, *et al.* Microwave assisted combustion synthesis of nanocrystalline yttria and its powder characteristics. *Powder Technol* 2009, **191:** 309–314.

[19] Dasgupta N, Krishnamoorthy R, Jacob KT, Glycol – nitrate combustion synthesis of fine sinter-active yttria. *Inorg Mater* 2001, **3:** 143–149.

[20] Back M, Massari A, Boffelli M, *et al.* Optical investigation of Tb^{3+}-doped Y_2O_3 nanocrystals prepared by Pechini-type sol–gel process. *J Nanopart Res* 2012, **14:** 792.

[21] Seaverson LM, Luo SQ, Chien PL, *et al.* Carbonate Associated with Hydroxide Sol-Gel Processing of Yttria:. An Infrared Spectroscopic Study. *J Am Ceram Soc* 1986, **69:** 423–429.

[22] Rulison AR, Flagan RC, Synthesis of Yttria Powders by Electrospray Pyrolysis, *J. Am Ceram Soc*1994, **77:** 3244–3250.

[23] Dai Z, Liu Q, Toci G, *et al.*Fabrication and laser oscillation of Yb:Sc_2O_3 transparent ceramics from co-precipitated nano-powders. *Eur Ceram Soc* 2018, **38:** 1632–1638.

[24] Wen XH, Xvudong L, Guoxiang, Synthesis of yttria nanopowders for transparent yttria ceramics. *Opt. Mater* 2006, **29:** 239–245.

[25] Danelska A,Ulkowska U, Socha PR, *et al.* Surface properties of nanozirconia and their effect on its rheological behaviour and sinterability. *Eur Ceram Soc* 2013, **33:** 1875–1883.

[26] Pradhan M, Kapur PC, *et al.* Effect of powder dispersion on sintering behavior and mechanical properties of nanostructured 3YSZ ceramics. *Ceram Int* 2012, **38:** 2835–2843.

[27] Moreno R. Colloidal Processing of Ceramic-Ceramic and Ceramic-Metal Composites. *Adv Appl Ceram* 2011, **225:** 147–159.

[28] Sun Y, Shimai S, Peng X, *et al.* Fabrication of transparent Y_2O_3 ceramics via aqueous gelcasting. *Ceram Int* 2014, **40:** 8841–8845.

[29] Santos SC, Acchar W, Yamagata C, *et al.* Yttria nettings by colloidal processing, *Eur Ceram Soc* 2014, **34:** 2509–2517.

[30] Xie Z, Ma J, Xu Q, *et al.* Effects of dispersants and soluble counter-ions on aqueous dispersibility of nano-sized zirconia powder. *Ceram Int* 2004, **30:** 219–224.

[31] Uchikoshi T, Hisashige T, Sakka Y. Stabilization of Yttria Aqueous Suspension with Polyethylenimine and Electrophoretic Deposition. *J Ceram Soc* 2002, 110: 840–843.

[32] Mouzon J, Glowacki E, Odén M. Comparison between slip-casting and uniaxial pressing for the fabrication of translucent yttria ceramics. *J Mater Sci* 2008, **43:** 2849–2856.

[33] He J, Li X, Zhu Q, *et al.* Dispersion of nano-sized yttria powder using triammonium citrate dispersant for the fabrication of transparent ceramics. *Ceram In*t 2016, **42:** 9737–9743.

[34] Jin L, Mao X, Wang S, *et al.*M. Dong, Optimization of the rheological properties of yttria suspensions. *Ceram Int* 2009, **35:** 925–927.

[35] Kruk A. Optical and structural properties of arc melted Ce or Pr – doped Y_2O_3 transparent ceramics. *Ceram Int* 2017, **43:** 16909–16914.

[36] Zhidkov IS, Maksimov RN, Kukharenko AI, *et al.*, Effect of post-annealing in air on optical and XPS spectra of Y_2O_3 ceramics doped with CeO_2. *Mendeleev Commun* 2019, **29:** 102–104.

[37] Mendelson ME. Average Grain Size in Polycrystalline Ceramics. *J Am Ceram Soc*1969, 52443–446.

[38] Khajelakzay M, Shoja Razavi R, Barekat M, *et al.* Synthesis of Yttria Nanopowders by Two Precipitation Methods and Investigation of Synthesis Conditions. I*nt J Appl Ceram. Technol* 2016, **13:** 209–218.

[39] Wang N, Zhang X, Bai Z, *et al.* Carbonate-precipitation synthesis of Yb^{3+}:Y_2O_3 nanopowders and its characteristics. *Powder Technol* 2010, **203:** 458–461.

[40] Li N, Ã KY. Journal of Solid State Chemistry Controlling the morphology of yttrium oxide through different precursors synthesized by hydrothermal method. *J Solid State Chem* 2008, **181:** 1738–1743.

[41] Srinivasan R, Yogamalar NR, Elanchezhiyan J, *et al.* Structural and optical properties of europium doped yttrium oxide nanoparticles for phosphor applications. *J Alloys Compd* 2010, **269:** 472–477.

[42] Muresan L, Popovici E, Grecu R, *et al.* Studies on the synthesis of europium activated yttrium oxide by wet-chemical method 1 . Influence of precursor quality on phosphor photoluminescence properties. *J Alloys Compd* 2009, **471:** 421–427.

[43] Huang Z, Sun X, Xiu Z, *et al.* Precipitation synthesis and sintering of yttria nanopowders. *Mater Lett* 2004, **58:** 2137–2142.

[44] K. Holmberg, Handbook of Applied Surface and Colloid Chemistry. New York (U SA) Emerald Group Publishing Limited,2002.

[45] Zorenko Y,Gorbenko TV, Zych E, *et al.* Luminescence properties of $Y_3Al_5O_{12}$:Ce nanoceramics. *J Lumin* 2011,**131:** 17–21.

[46] Borlaf M, Frankowska M, Kubiak WW, *et al.* Strong photoluminescence emission at low dopant amount in YAG:Ce and YAG:Eu phosphors. *Mater. Res. Bull.* 2018, **100:**413–419.

[47] Wang L, Zhao F, Zhuang J, *et al.* A facile route to Ce^{3+}-doped Y_3Al_5O 12 phosphors and their photoluminescent properties. *Mater Lett* 2014, **120:** 163–165.

[48] Osipov VV, Ishchenko AV, Maksimov RN, *et al.* Fabrication, optical and scintillation properties of transparent YAG:Ce ceramics. *Opt. Mater*. 2017, **71:** 98–102.

[49] Raukas M, Konrad A, Mishra KC, Luminescence in nano-size Y_2O_3:Ce. *J Lumin* 2007, **123:** 773–775.

[50] Li HL, Liu XJ, Huang LP, Fabrication of Transparent Cerium-Doped Lutetium Aluminum Garnet (LuAG:Ce) Ceramics by a Solid-State Reaction Method. *J Am Ceram Soc* 2005, **88:** 3226–3228.

[51] Nikl M, Mihoková E, Mareš JA, *et al.* Traps and timing characteristics of LuAG:Ce^{3+} scintillator. *Phys Status Solidi A* 2000, **181:** 10–12.

Figures

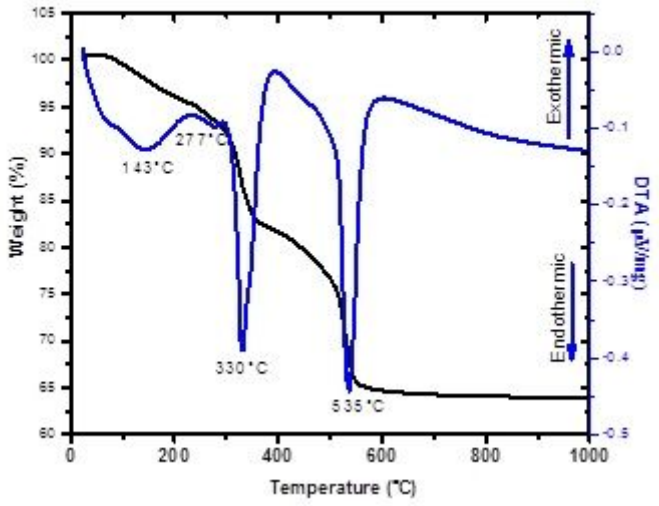

Figure 1

DSC/TGA data of the precipitated hydroxide precursor.

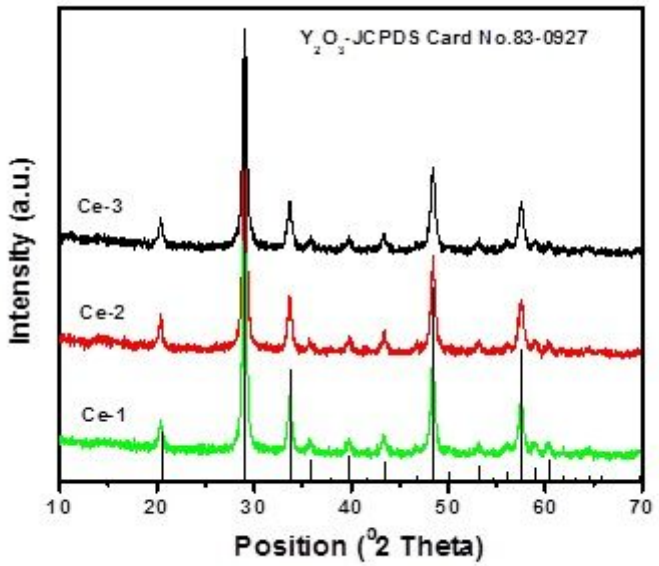

Figure 2

XRD pattern of prepared Ce3+ doped Y2O3 powder calcined at 700 °C.

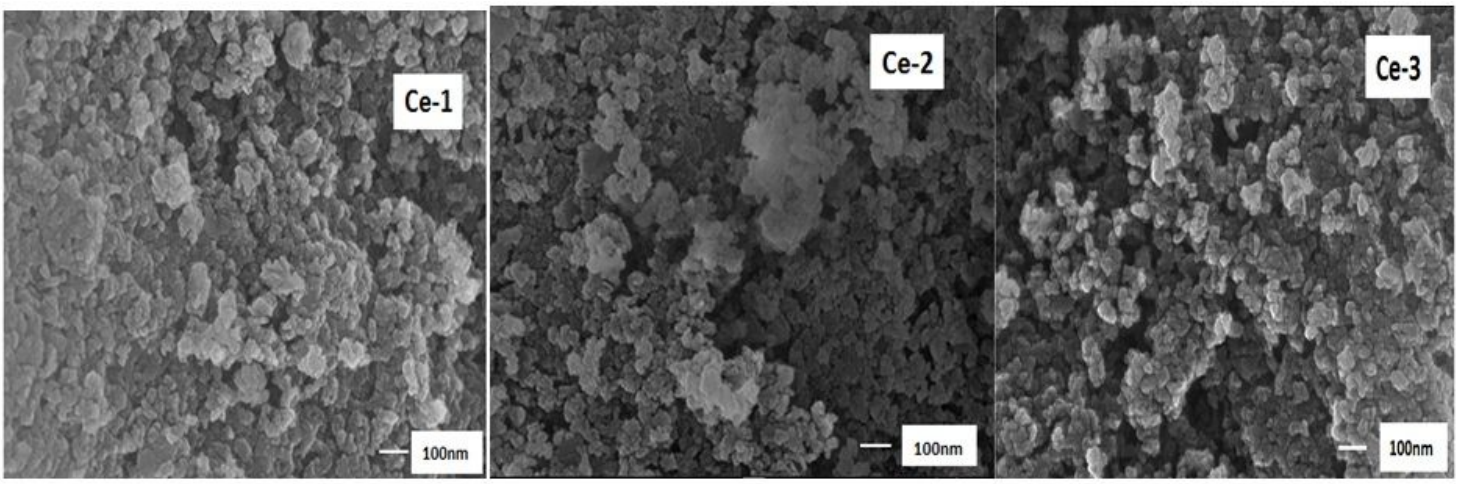

Figure 3

SEM micrograph of the synthesised Ce3+ doped Y2O3 powders, Ce-1) 0.001 mol % Ce, Ce-2) 0.005 mol % Ce, Ce-3) 0.01 mol % Ce.

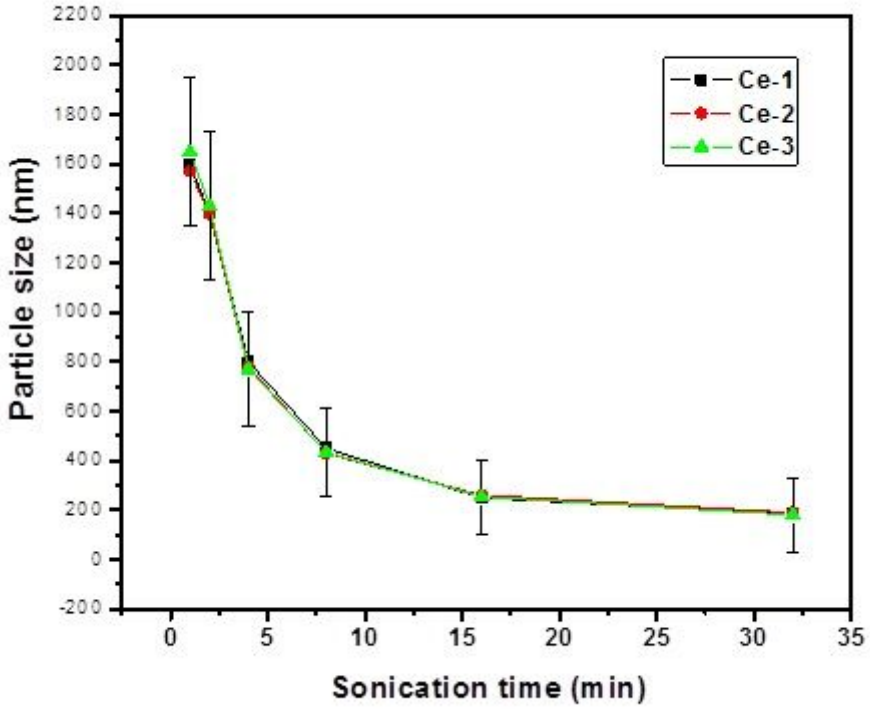

Figure 4

The change of particle size distribution of the ceria doped yttria nanoparticles with the sonication time.

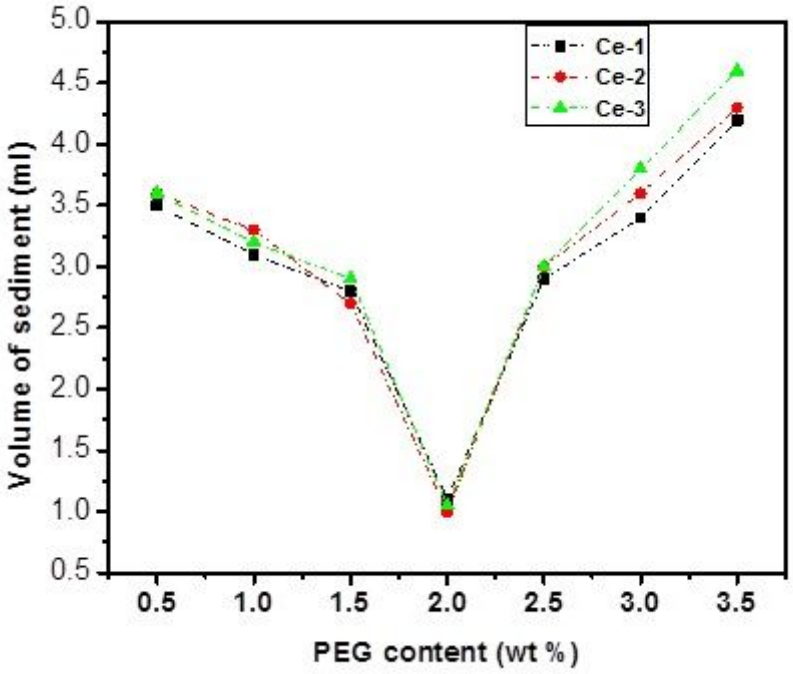

Figure 5

Sedimentation volume at various PEG contents.

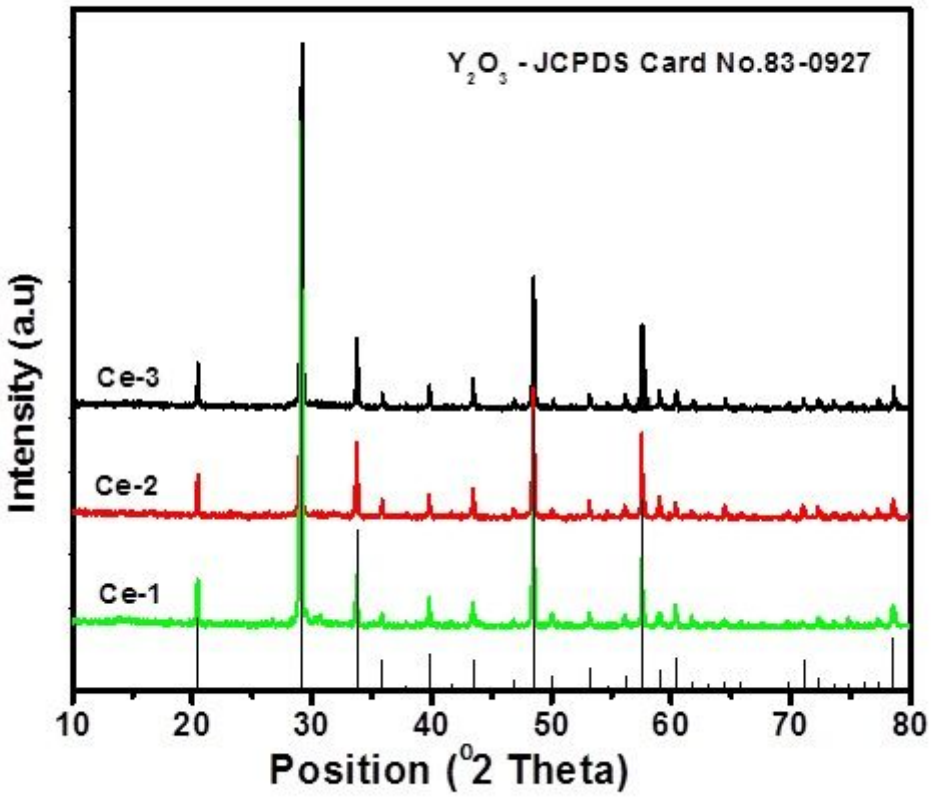

Figure 6

XRD patterns of Y2O3:Ce3+ ceramics sintered at 1550 °C for 3 h.

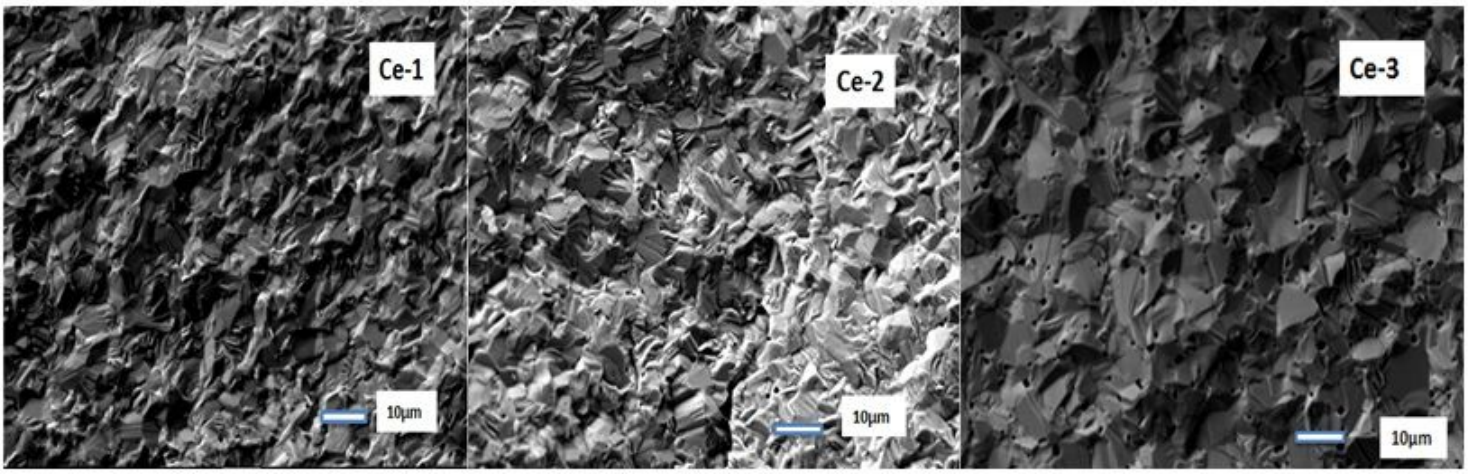

Figure 7

Fracture surfaces of sintered Ce3+ doped Y2O3 powder, Ce-1) 0.001 mol % Ce, Ce-2) 0.005 mol % Ce, Ce-3) 0.01 mol % Ce.

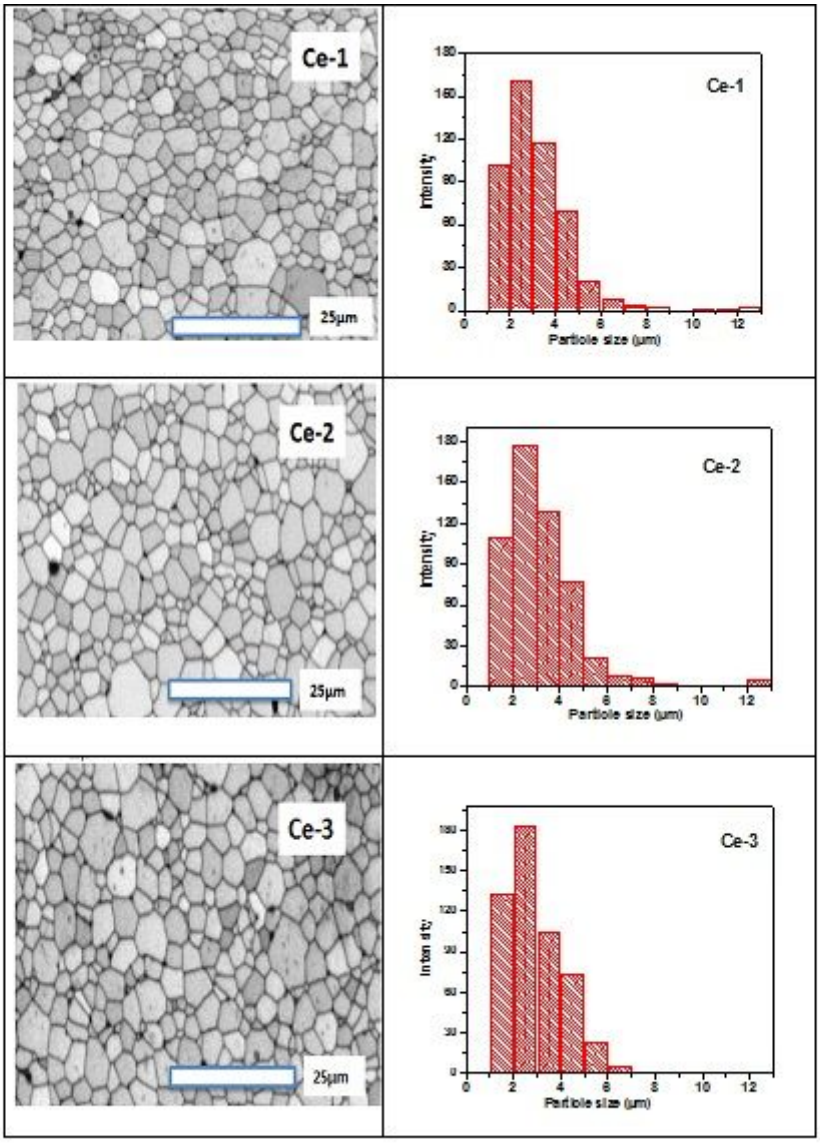

Figure 8

The EBSD image of sintered samples and particle size distributions of Ce3+ doped Y2O3 ceramics, Ce-1) 0.001 mol % Ce, Ce-2) 0.005 mol % Ce, Ce-3) 0.01 mol % Ce.

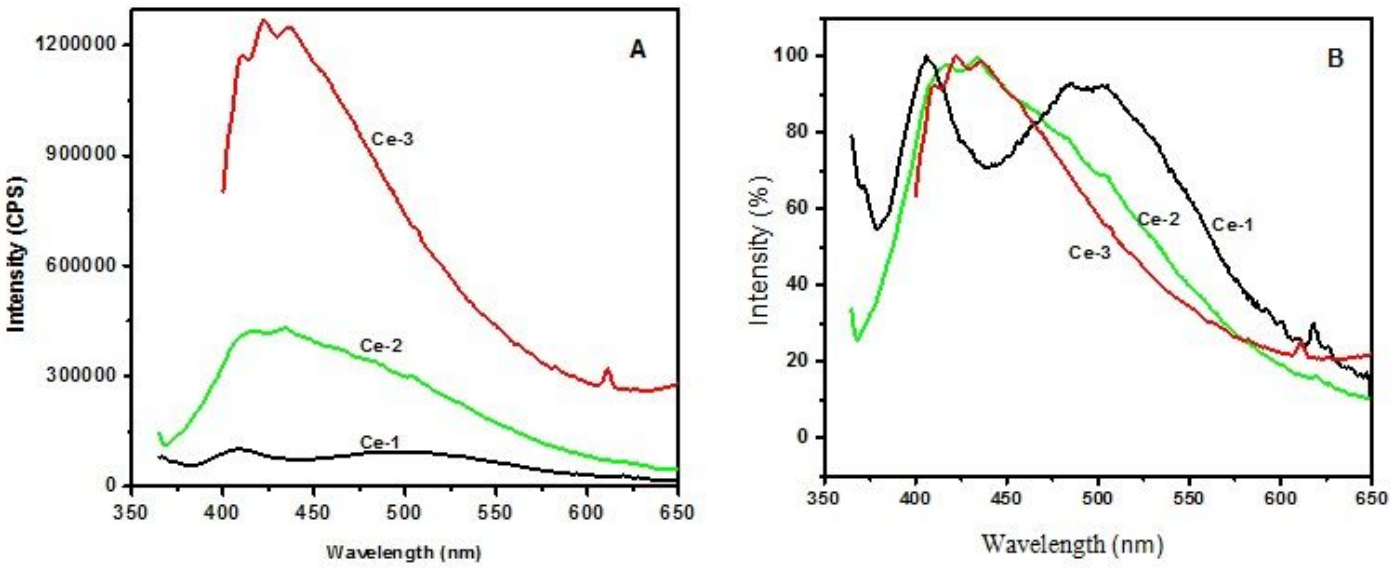

Figure 9

Shows the emission spectra of Y2O3:Ce3+ ceramics sintered at 1550 °C, A) Emission spectrum of Y2O3:Ce3+,B) Normalized emission of Y2O3:Ce3+